Dynamic Compression of Enstatite[1]

THOMAS J. AHRENS AND EDWARD S. GAFFNEY

Seismological Laboratory
California Institute of Technology, Pasadena 91109

New shock wave data for Bamle enstatite $(Mg_{0.86},Fe_{0.14})SiO_3$ in the range from 60–480 kb indicate a Hugoniot elastic limit of 67 ± 10 kb and a possible phase-transition–produced shock front of 135 ± 10 kb amplitude. Above the latter shock pressure, states in a mixed-phase regime are achieved up to ~350 kb, above which the Hugoniot states are believed to represent the equation of state of a shock-induced phase, probably having the majorite (garnet) structure with a zero-pressure density of ~3.67 g/cm³. The present data, representing the high-pressure phase, agree closely with those of R. G. McQueen, S. P. Marsh, and J. N. Fritz above 610 kb for a Stillwater bronzitite of similar mineralogy. It is suggested that the formation of majorite from enstatite in naturally impacted rocks and meteorites requires dynamic pressures of at least ~135 kb.

Shock-wave equations of state for pyroxenes are of considerable importance, both for the understanding of shock metamorphism processes in lunar gabbros and basalts and for determining the constitution of terrestrial planetary mantles. The proposed presence of 15 to 18% orthopyroxene and clinopyroxene in the pyrolite and 40% pyroxene in the eclogite earth upper-mantle models of *Clark and Ringwood* [1964] and from 40 to 80% pyroxene in the earth's lower mantle [*Birch*, 1964; *Anderson et al.*, 1971] provides ample motivation for the study of this mineral. The present detailed Hugoniot measurements were carried out on single-crystal Bamle orthoenstatite $(Mg_{0.86},Fe_{0.14})SiO_3$ to 480 kb. Previously ultrasonic data were reported by *Rhyzhova et al.* [1966] for a slightly porous sample and by *Kumazawa* [1969] for a gem-quality sample. Shock-compression measurements on two enstatite-bearing rocks to pressures of ~1.1 Mb by *McQueen et al.* [1967] and similar data by *Trunin et al.* [1965] indicated anomalously large compressions for the higher pressure states; however, their results have been variously interpreted in later papers by other workers. The present study was carried out on a single-phase enstatite in order to delineate the phase-change regime and to obtain the equation-of-state data for the shock-induced phase.

Specimen Material

A series of disk-shaped samples were cut from several large single crystals of orthoenstatite (Bamle, Norway) purchased from Ward's Natural Science Establishment. The cylindrical disk axes were oriented to within ±3° of (001) using the external crystal faces. After inspection by radiography, samples having no obvious inclusions and only minor cracks were retained. These remaining samples, which were light brown and translucent, were surface ground to a nominal thickness of 4.7 mm. The planar surfaces were machined flat and parallel to 0.008 mm.

Thin sections of this material were examined by Rex V. Gibbons. The specimen material had a negative optical sign, indicating that it contains more Fe^{++} than $En_{0.89}$. A measurement of the index of refraction n_x of 1.6820 ± 0.002 (white light) indicated a stoichiometry of $En_{0.86 \pm 0.015}$. A value of n_x (Na light) gives a value of 1.6695 ± 0.001, indicating stoichiometry of $En_{0.86}$ [*Deer et al.*, 1966]. Microprobe analysis by A. Albee and A. Chodos gave a stoichiometry of $(Mg_{0.86}, Fe_{0.14}, Ca_{0.005}, Al_{0.003})Si_{0.99}O_3$. A second analysis gave a similar result for the major elements but also indicated some manganese was present ($Mn_{0.01}$). On the basis of these analyses we conclude that the composi-

[1] Contribution 1956, Division of Geological and Planetary Sciences, California Institute of Technology. Lunar Science Institute Contribution 57.

tion of our samples can be closely described by the formula $(Mg_{0.86}, Fe_{0.14})SiO_3$. Hence the mineral is actually bronzite rather than enstatite. This Fe^{++}/Mg^{++} ratio, 0.16, is close to the ratio that is inferred to exist in the earth's upper mantle [*Anderson*, 1967*b*]. Taking a zero-pressure density for orthoferrosilite of 3.982 g/cm³ [*Akimoto et al.*, 1965] and assuming an ideal $(Mg, Fe)SiO_3$ solid solution, a theoretical zero-pressure crystal density of 3.308 g/cm³ is calculated for Bamle enstatite. A Debye-Scherrer X-ray determination gave the lattice parameters $a_0 = 18.216 \pm 0.039$, $b_0 = 8.826 \pm 0.019$, and $c_0 = 5.210 \pm 0.011$. Assuming a molecular weight of 104.824 yields an X-ray density of 3.325 g/cm³. Initial densities of our samples were obtained by the water-immersion method and by separately measuring the sample volume and mass. These methods agreed to within ± 0.005 g/cm³, which is the uncertainty we assign to the densities listed in Table 1. By using the above theoretical crystal density, we calculate initial porosities of from 1 to 3%.

EXPERIMENTAL DETAILS

Hugoniot data were obtained using the projectile-impact method and streak-camera recording system described in *Ahrens et al.* [1971]. A 40-mm-diameter lexan plastic projectile, carrying a 2.5-mm-thick tungsten or tungsten alloy (90% W, 6% Ni, 4% Cu) flyer plate, was accelerated in 6 meters to speeds of 1 to 2.5 km/sec with a smooth bore propellant gun. During the final 1 meter of travel, the projectile velocity is determined by allowing the flyer plate front surface to intersect 3 fixed laser beams. On impact with the target, a pin switch is actuated. These events turn 0.1 μsec resolution time-interval counters on and off. The pin switch also triggers the sweep of an image-converter streak camera that in turn determines shock velocity.

Because we have previously observed a 1 to 3% increase in projectile speed during the last meter of projectile flight, an extra pair of pin switches detects projectile arrival times during the final 1 mm of travel prior to impact. This redundant time-interval measurement is made using an Eldorado Model 796 unit that has a resolution better than 1 nsec. The impact velocity is determined by analytically fitting a linear velocity-distance function to the data. To weight the data in this procedure, we assume the significant errors to be the time-interval uncertainties of ± 0.15 μsec for the laser observations and pin-distance errors of ± 0.005 mm for the final pin measurement. Except for shots 162, 147, and 152, for which complete velocity data were not obtained, the uncertainties shown in Table 1 are the average of the residuals.

Shock velocities are determined from the initial specimen thicknesses and the travel times recorded by the streak camera. Since the streak-camera writing rate at any point on the film is known to within $\pm 0.25\%$ (by the method described in *Ahrens et al.* [1971]), the principal errors in shock velocity arise from the inherent sample inhomogenities that produce variations in travel time along the line of the observing slit. (Maximum errors are quoted in Table 1.) Corrections of the shock travel time for tilt, both along, and perpendicular to, the slit direction were applied. The shock tilt perpendicular to the slit direction was measured using arrival times observed through a second, auxiliary slit that views an image displaced 5 mm from the main slit.

Inclined mirrors mounted on the sample were used to determine arrival times of successive shock fronts as well as the associated velocities imparted to the free surface.

Final shock states are calculated using the impedance-match method. On impact of the flyer plate with the target assembly, the shock state in the 1.5-mm-thick driver plate, on which the sample disks are mounted, is assumed to be that of the Hugoniot state, corresponding to one-half the projectile velocity. The flyer and driver plates are both made of either tungsten or tungsten alloy. Because we observed variations in the initial density of the tungsten alloy (arising from variable porosity) three different Hugoniot curves for this material were employed for impedance-matching purposes depending on initial density. These 'standard' Hugoniots were constructed by assuming that a 'simple locking' [*Linde and Schmidt*, 1966] occurs to a pressure-volume state defined by the mass-weighted sum of the Hugoniot specific volumes of the tungsten alloy constituents. Principal Hugoniots for W, Cu, and Ni given in *McQueen et al.* [1970] were used

TABLE 1. Hugoniot Data for Bamle Enstatite

Shot No.	Driver Plate[a]	Projectile Velocity, km/sec	Initial Density, g/cm³	Initial Thickness, mm	Shock Velocity, km/sec	Particle Velocity, km/sec	Shock Pressure, kb	Density, g/cm³
				Initial Shock State				
98	1	0.950 ±0.030	3.288	4.729	7.841[b] ±0.062 6.83[c] ±0.12	0.342[b] ±0.02	77 ± 6[b]	3.461[b] ±0.010
132	1	1.074 ±0.006	3.282	4.727	7.739[b] ±0.070	0.224[b] ±0.02	57 ± 6[b]	3.380[b] ±0.005
146	1	1.267 ±0.013	3.290	4.676	7.94[b] ±0.34 7.35[c] ±0.28	0.571[c] ±0.027	138 ± 12[c]	3.567[c] ±0.020
100	1	1.574 ±0.005	3.287	4.729	7.599[b] ±0.031	0.268[b] ±0.026	67 ± 7[b]	3.407[b] ± .007
142	2	1.682 ±0.035	3.276	4.671	7.325[c] ±0.028			
99	1	1.677 ±0.03	3.298	4.727	7.907[b] ±0.094 7.247[c] ±0.060			
134	1	1.958 ±0.02	3.288	4.669	7.903[b] ±0.070 7.247[c] ±0.060	0.532[c] ±0.047	127 ± 12[c]	3.549[c] ±0.020
118	0	1.907 ±0.031	3.287	4.671	7.165[c] ±0.077	0.600[c] ±0.046	141 ± 12[c]	3.587[c] ±0.024
130	0	2.065 ±0.010	3.278	4.671	7.47[b] ±.02			
167	3	2.189 ±0.060	3.291	4.671	7.468[b] ±0.027			
162	2	2.22 ±0.1	3.294	4.729	7.726[b] ± .030			
147	1	2.35 ±0.1	3.287	4.674	7.56[b] ±0.12			
160	1	2.443 ±0.092	3.282	4.676	*d*			
152	1	2.48 ±0.10	3.293	4.674	7.995[b] ±0.033			
166	3	2.52 ±0.02	3.288	4.676	7.950[b] ±0.042			
				Final Shock State				
98	1	0.950 ±0.030	3.288	4.729	6.363 ±0.064	0.698 ±0.027	151 ± 16	3.678
132	1	1.074 ±0.006	3.282	4.727	6.158 ±0.045	0.793 ±0.007	171 ± 11	3.738
146	1	1.267 ±0.013	3.290	4.676	6.807 ±0.027	0.925 ±0.013	217 ± 23	3.78
100	1	1.574 ±0.005	3.287	4.729	6.860 ±0.028	1.166 ±0.007	269 ± 14	3.945 ±0.062
142	2	1.682 ±0.035	3.276	4.671	6.735 ±0.028	1.281 ±0.019	283 ± 7	4.045 ±0.021
99	1	1.677 ±0.03	3.298	4.727	7.109 ±0.054	1.247 ±0.031	291 ± 7	3.995 ±0.019
134	1	1.958 ±0.02	3.288	4.669	6.965 ±0.031	1.465 ±0.022	340 ± 27	4.151
118	0	1.907 ±0.031	3.287	4.671	7.015 ±0.055	1.444 ±0.031	336 ± 30	4.131

TABLE 1 (*Continued*)

Shot No.	Driver Plate[a]	Projectile Velocity, km/sec	Initial Density, g/cm³	Initial Thickness, mm	Shock Velocity, km/sec	Particle Velocity, km/sec	Shock Pressure, kb	Density, g/cm³
130	0	2.065 ±0.010	3.278	4.671	6.82 ±0.15	1.561 ±0.016	349 ± 8	4.252 ±0.035
167	3	2.189 ±0.060	3.291	4.671	6.917 ±0.042	1.741 ±0.052	396 ± 14	4.399 ±0.048
162	2	2.22 ±0.1	3.294	4.729	7.257 ±0.029	1.743 ±0.081	397 ± 20	4.272 ±0.060
147	1	2.35 ±0.1	3.287	4.674	7.165 ± .086	1.770 ±0.084	417 ± 23	4.365 ±0.082
160	1	2.443 ±0.092	3.282	4.676	7.052 ±0.070	1.850 ±0.078	428 ± 21	4.449 ±0.073
152	1	2.48 ±0.10	3.293	4.674	7.309 ±0.059	1.861 ±0.083	448 ± 23	4.418 ±0.067
166	3	2.52 ±0.02	3.288	4.676	7.391 ±0.045	1.987 ±0.019	483 ± 8	4.497 ±0.022

[a] 0, 1, and 2 refer to 16.6, 16.8, and 17.0 g/cm³ density tungsten alloy; 3 is pure (19.3 g/cm³) tungsten.
[b] Hugoniot elastic limit shock (HEL).
[c] Possible transition shock state.
[d] Precursor to final shock state not detected.

for calculating the Hugoniot of the alloy and of pure W in the pressure-volume plane. By using the Rankine-Hugoniot equations the Hugoniot data were cast into the pressure-particle velocity (p–u) plane. The curves for tungsten and tungsten alloy could be closely fitted by the polynomial

$$p = a_1u + a_2u^2 + a_3u^3 \qquad (1)$$

The coefficients used in our analysis are given in Table 2.

EXPERIMENT RESULTS

The results of a series of fifteen Hugoniot experiments with final shock states between 151 and 483 kb are summarized in Figure 1. In all but one (shot 160) of the experiments, a very distinct shock arrival prior to the main shock was observed, either as a partial loss of reflectivity of the flat mirrors on the specimen free surface, or as evidenced by an initial low-velocity motion of the free surface, detected by the inclined mirror [*Ahrens et al.*, 1971]. Complete loss of flat-mirror reflectivity occurred within 15 nsec of the onset of the final shock-state free-surface velocities as determined by the extinction of light from the inclined mirror.

In eleven of these experiments, first shock velocities ranging from 7.5 to 8.0 km/sec (average 7.78 km/sec) were measured. Because these shock velocities are nearly equal to the longitudinal elastic velocity along (001) measured by *Kumazawa* [1969] of 7.853 km/sec and the 7.865 ± 0.015 km/sec measured in our laboratory, we infer that this shock front corresponds to an elastic precursor. The observed variation probably reflects differences in porosity and crystal orientation of the different samples.

Free-surface velocities associated with this

TABLE 2. Hugoniots of Driver Materials, Pressure-Particle Velocity Curves

Material	Designation (Table 1)	Polynomial Coefficients (Equation 1)		
		a_1, kb sec/km	a_2, kb sec²/km²	a_3, kb sec³/km³
Tungsten, 19.3 g/cm³	3	767.3	276.5	−34.7
Tungsten alloy, 16.6 g/cm³	0	429.3	502.5	−125.2
Tungsten alloy, 16.8 g/cm³	1	491.5	451.7	−105.3
Tungsten alloy, 17.0 g/cm³	2	566.8	373.6	−69.9

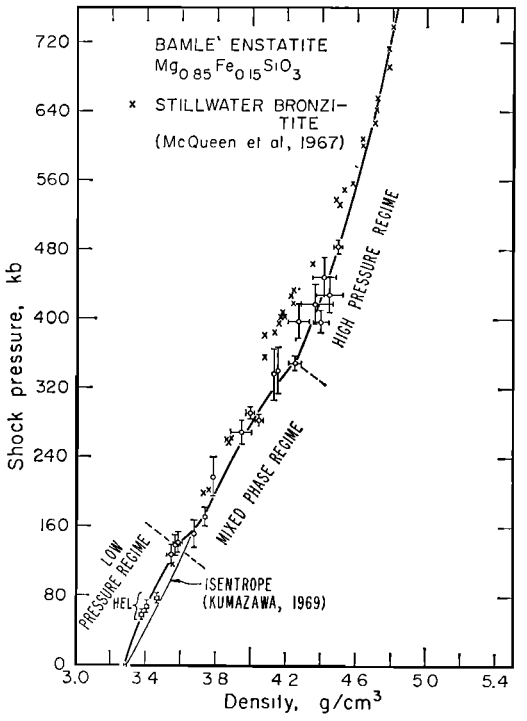

Fig. 1. Hugoniot data for Bamle enstatite. Ultrasonic measurements of *Kumazawa* [1969] and an assumed value of $dK/dP = 5$ are used to construct theoretical principal isentrope for low-pressure (pyroxene) phase. Maximum experimental errors are indicated.

shock arrival were measured in three shots. Assuming the free-surface velocity is twice the particle velocity [*Walsh and Christian,* 1955] yields shock pressures for the Hugoniot elastic limit (HEL) of 67 ± 10 kb.

At low final shock stress, a second early shock arrival, which may represent the onset of a phase transition, was observed in four experiments. Excluding shot 98, this apparent wave travels at speeds of between 7.2 and 7.4 km/sec. Three measurements of free-surface velocity associated with this shock yield shock pressures of 135 ± 10 kb. Although the meaning of this arrival is not clear to us, the fact that the final Hugoniot states above a level of ~150 kb lie at a greater density than the final states we infer for the enstatite isentrope, centered at STP, supports the above interpretation. The enstatite isentrope was calculated by using Kumazawa's 1.05 Mb bulk modulus and an assumed $(dK/dp)_s$ of 5. Different values of $(dK/dp)_s$ will not alter the curve appreciably.

At higher shock-stress levels, extending to the vicinity of 340 kb, the Hugoniot states appear to represent states that are a mixture of enstatite and a high-pressure phase. The data of *McQueen et al.* [1967] for Stillwater bronzitite lie at appreciably higher pressures, at a given density, in this interval. The difference probably arises from different points on the shock-wave profile being used to indicate shock arrivals. Our final state arrival times are picked to coincide with the time when the specimen free-surface velocity achieves its final value. These times are later than those of *McQueen et al.* [1967]; hence, at a given particle velocity, our final shock velocities are lower and the compressions are greater.

The seven Hugoniot points, above the mixed-phase region, are thought to represent states for the wholly transformed material. The data agree well with those for the Stillwater material in the 600 to 1100 kb range.

Shock-Induced High-Pressure Phase

In addition to these data, several petrologic results have been recently published bearing on the question of the nature of the shock-induced phase in pyroxene. Static high-pressure and high-temperature phase equilibrium quenching experiments on pyroxenes in the ranges $FeSiO_3$ to $Mg_{0.75}Fe_{0.25}SiO_3$ and $FeSiO_3$ to $Fe_{0.7}Mg_{0.3}SiO_3$ were studied by *Ringwood and Major* [1968] and *Akimoto and Syono* [1970]. Both groups observed that these solid-solution pyroxenes reacted to form a stoichiometric mixture of stishovite (SiO_2) and ringwoodite (spinel structure, $(Fe, Mg)_2SiO_4$) on recovery from (static) high pressure (Figure 2).

We have carried out a series of thermochemical calculations in order to explore the temperatures and pressures required to produce the above observed transformation in the more magnesium-rich pyroxene similar to the composition of $(Mg_{0.86},Fe_{0.14})SiO_3$ according to the formula

$$(Mg, Fe)\,SiO_3 \text{ (clinopyroxene)} \rightarrow \tfrac{1}{2}(Mg, Fe)_2SiO_4 \text{ (ringwoodite)} + \tfrac{1}{2}SiO_2 \text{ (stishovite)} \quad (2)$$

A second reaction investigated was

2(Mg, Fe) SiO_3 (clinopyroxene)

$\rightarrow$ 2 (MgO (periclase), 2 FeO (wüstite))

$+ SiO_2$ (stishovite) (3)

Our calculations were carried out assuming that we are dealing with only a two-phase system, and thus the reaction products are assumed to behave as a single phase, with thermochemical and equation-of-state properties equal to the appropriate molar average. Ideality in the solid solution is also assumed. This assumption has been shown to be approximately valid in the case of the olivine-spinel transformations [*Akimoto*, 1970] and in the case of reaction 2, as demonstrated by the present calculational results.

In order to calculate the reaction pressures at various temperatures for the Mg-Fe end members of reactions listed above, it is convenient to employ standard enthalpies and entropies under standard temperature and pressure conditions for these compounds. For $MgSiO_3$ (clinopyroxene), and for the oxides FeO, MgO and SiO_2 (stishovite), these data as well as the appropriate molar volumes are listed in *Robie and Waldbaum's* [1968] recent compilation of thermochemical data. Thermochemical data for the spinels, Fe_2SiO_4 and Mg_2SiO_4, (γ phase) have been calculated by *Mao* [1967]. For $FeSiO_3$ (ferrosilite) the *P-T* phase diagram for the reactions

$FeSiO_3$ (orthopyroxene)

$\rightarrow FeSiO_3$ (clinopyroxene) (4)

and the calculated phase line

2 $FeSiO_3$ (clinopyroxene)

$\rightarrow Fe_2SiO_4$ (spinel) $+ SiO_2$ (coesite) (5)

which have been studied by *Akimoto et al.* [1965], were used to calculate values for the standard entropy and enthalpy of clinoferrosilite. The resulting values were: 0.022 kcal/mole °K and $-$ 2.63 kcal/mole, respectively.

At a temperature T, the transformation pressure p_i^T for a given end member may be calculated from

$$\Delta G_i^{T,p} = \Delta H_i^T - T\Delta S_i^T = -\int_0^{p_i^T} (V_i^2 - V_i^1)\, dp \quad (6)$$

Here i indicates the end member component (1 or 2) of a solid-solution series, the superscripts 1 and 2 refer to the high-pressure and low-pressure phase, respectively, and ΔH_i^T and ΔS_i^T are the differences in enthalpy and entropy at zero-pressure and at temperature T. The integral in (6) is along the isotherm at temperature T. Equation 6 must be solved for p_i^T for each component $i = 1, 2$ for each tem-

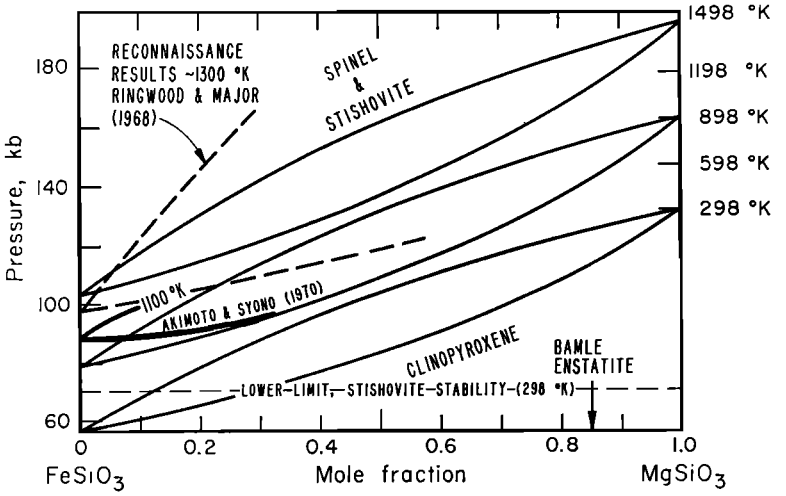

Fig. 2. Theoretical phase diagram for breakdown of (Mg, Fe) pyroxene to (Mg, Fe)$_2SiO_4$ (ringwoodite) + SiO_2 (stishovite). Comparison of theoretical diagram with experimental data of *Akimoto and Syono* [1970] indicates the approximate validity of ideal mixing assumption.

perature. For a two-component, ideal mixing solid-solution system, the mole fractions of component 1, in the low-pressure phase X_{11}, in equilibrium with the high-pressure phase of composition X_{21}, are given by

$$X_{11} = \frac{\exp(\Delta G_1^{T,p}/nRT)[\exp(\Delta G_2^{T,p}/nRT) - 1]}{\exp(\Delta G_2^{T,p}/nRT) - \exp(\Delta G_1^{T,p}/nRT)} \quad (7)$$

$$X_{21} = \frac{\exp(\Delta G_2^{T,p}/nRT) - 1}{\exp(\Delta G_2^{T,p}/nRT) - \exp(\Delta G_1^{T,p}/nRT)}$$

Here n is the number of atoms in each molecule that can enter the solid solution. In the present calculation, n is assumed to be 2; its actual value will depend on the degree of Mg^{++}–Fe^{++} ordering in the solid solution. Solution of equation 6, which determines the phase lines of the end members in p, T space, depends on knowledge of the enthalpies and entropies as a function of temperature. p_i^T in (6) and (8) depends on knowledge of the p-V isotherms at various temperatures. A calculational method that has been used to determine these quantities is outlined below.

At each temperature it is assumed that the pressure-volume isotherms are given by the Birch-Murnaghan form of the isothermal equation of state. It is also assumed that the thermodynamic quantity

$$(\partial p/\partial e)_v = \gamma/V \quad (8)$$

is constant for each material and has the value observed, or calculated, at standard temperature and pressure [*Walsh and Christian*, 1955]. Here γ is the Grüneisen parameter and e is the internal energy. This assumption and another (discussed below) concerning the variation of $(\partial K_T/\partial p)_T$ for different materials are made because a complete knowledge of the pertinent equations of state is, in general, lacking.

The temperature dependence of C_v, the specific heat at constant volume, was assumed to be given by a Debye theory. The Debye temperature at each phase is estimated from its standard enthalpy or from specific heat data. To obtain an estimate of the variations in bulk modulus with temperature, we have applied an empirical observation of *Anderson* [1967*a*]. In the case of oxides and silicates Anderson observed that the variation of the bulk modulus with volume is similar when the volume change is produced by either compression or changes in temperature. Specifically, data for ten minerals listed by Anderson suggests the relation

$$\left(\frac{\partial \ln K_T}{\partial \ln \rho}\right)_p \cong \left(\frac{\partial \ln K_T}{\partial \ln \rho}\right)_T + 0.85 \quad (9)$$

Taking (12) as an equality, it follows that

$$\left(\frac{\partial K_T}{\partial T}\right)_p = -\alpha K_T\left[\left(\frac{\partial K_T}{\partial p}\right)_T + 0.85\right] \quad (10)$$

The properties of the various phases can be calculated numerically at a series of finite temperature increments as a function of temperature in the order given below. The change in volume is calculated from the coefficient of expansion α. At each successive temperature the value of α is revised by using the Grüneisan relation

$$\alpha = (\gamma/V)(C_p/K_s) \quad (11)$$

where K_s is the adiabatic bulk modulus and C_p is the specific heat at constant pressure. The change in the Debye temperature θ_D with changing volume is calculated from

$$\theta_D = \theta_0 \exp[\gamma(V_0 - V)/V_0] \quad (12)$$

which follows from the Debye model and the assumption regarding equation 8. A new value of C_p is calculated from the thermodynamic identity

$$C_p = C_v + \alpha^2 VTK_T \quad (13)$$

and the change in enthalpy and entropy due to the incremental temperature increase is then calculated for both end members, in their high-pressure and low-pressure phases.

Using the above procedure, the theoretical phase diagrams calculated for reactions 2 to 3 are shown in Figures 2 and 3.

The calculation for reaction 3, summarized in Figure 3, indicates that it takes a greater shock pressure, at least 180 kb at room temperature, than the 135 kb observed to produce the direct transformation of clinoenstatite to mixed oxide-type phase for a stoichiometry corresponding to Bamle enstatite. (The temperature rise due to shock compression and the small density and enthalpy differences between

the orthopyroxenes and clinopyroxenes can be neglected.)

The value of the zero-pressure density of a phase similar in density to the mixed oxides for the stoichiometry of Bamle enstatite is ~4.17 g/cm³. This is considerably higher than the Hugoniot results obtained in the high-pressure shots on the Bamle and Stillwater [*Ahrens et al.*, 1969; *McQueen et al.*, 1967] materials indicate.

In contrast to results for the transformation to the mixed-oxide–type phase, the calculated phase diagram for reaction 2 gives a transition pressure of approximately 120 kb. This lower limit is indicated in Figure 2 and is close to the onset of the pressure stability range of stishovite. The agreement with *Akimoto and Syono's* [1970] stability diagram near the $FeSiO_3$ stoichiometry is also indicated in Figure 2. The agreement with their results as well as *Ringwood and Major's* [1968] reconnaissance work is remarkably good considering our present meager knowledge of the properties of ferrosilite.

The results of the calculation of the *p-T* composition phase lines for reaction 2 may be interpreted literally as actually representing the breakdown reaction to stishovite and ringwoodite that may occur in enstatite under shock compression, or the calculation may be used as a guide to the density of a possible homogeneous phase produced in the shock experiments. Although we prefer the latter argument, *Wang* [1967] has inferred that the zero-pressure density, 3.71–3.83 g/cm³, obtained by analyzing the high-pressure portion of the McQueen et al. specimen of Stillwater bronzitite Hugoniot, represented the products of reaction 2. For similar composition to our specimens, this would have a zero-pressure density of ~3.80 g/cm³. A similar value for the zero-pressure density of the high-pressure phase, 3.77 g/cm³, was obtained by *Anderson and Kanamori* [1968]. These two analysts constrained the zero-pressure density and seismic parameter $(\partial P/\partial \rho)_s$ so as to satisfy a Birch-type velocity-density correlation and a seismic equation of state (SEOS) [*Anderson*, 1967*a*]. Later *Ahrens et al.* [1969] and *Davies and Anderson* [1971] used slightly different constants and data sets and

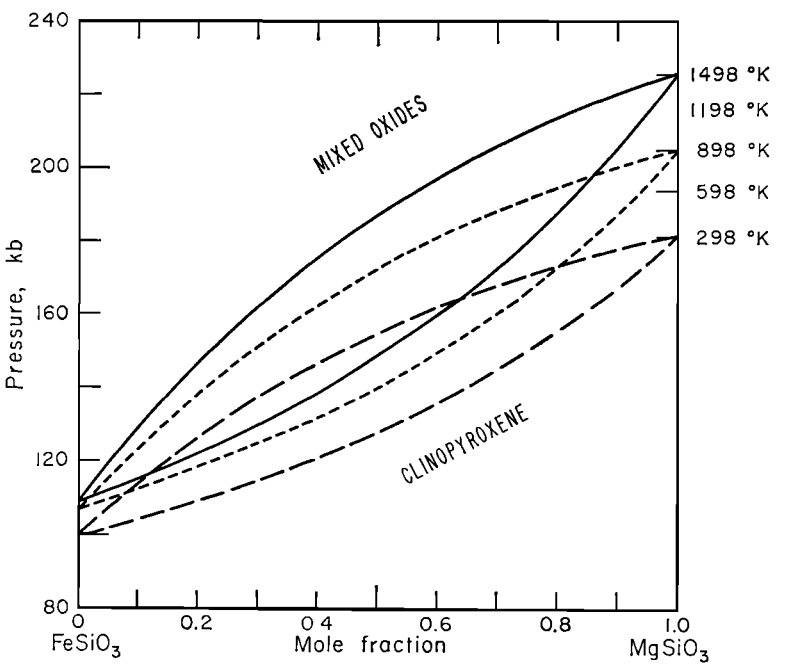

Fig. 3. Theoretical phase diagram for direct breakdown of (Mg, Fe) pyroxene to a phase having the properties of the mixed oxides. This reaction appears to take place at too high a pressure to account for the observed shock transition in enstatite.

applied the SEOS as a zero-pressure constraint to obtain zero-pressure densities of 3.74 and 3.33 g/cm^3, respectively. Both studies concluded that the high-pressure phase of Stillwater bronzitite represented the ilmenite structure. The denser perovskite structure was also considered by these authors and by *Gaffney and Ahrens* [1970] as a possible shock-induced phase.

Studies of shock-induced changes in terrestrial and lunar pyroxenes [namely, *James*, 1969; *Chao et al.*, 1970], although they demonstrated that decreases in the index of refraction, intense books of lamellas, and twinning occur, have yielded no clear incidence as to the crystallographic nature of the high-pressure phase that is inferred from the Hugoniot data.

Convincing evidence that the garnet structure can actually be produced by shock was reported by *Smith and Mason* [1970], who observed a new Mg, Fe garnet, majorite, which also contained some Al, in the Coorara meteorite. Unfortunately Smith and Mason could not distinguish Fe^{++} from Fe^{+++} in this material. The meteorite also contains, presumably, shock-induced ringwoodite [*Binns*, 1970]. On the basis of Smith and Mason's analysis for this garnet and their reported lattice parameter of 11.524 ± 0.002 A, a similar garnet with the stoichiometry of the Bamle enstatite is calculated to have a zero-pressure density of 3.67 g/cm^3. This is lower than either a theoretical ilmenite structure density of 3.85 g/cm^3 or a mixture of ringwoodite and stishovite with a density of 3.89 g/cm^3 for the Bamle stoichiometry. Analysis of the present seven high-pressure–phase data points for Bamle enstatite, when combined with seven data points of *McQueen et al.* [1967] in the range 601 to 718 kb, yields a zero-pressure density of 3.57 g/cm^3 and a bulk modulus 1.43 Mb for the raw Hugoniot. This result was obtained with the values $A = 0.0492$ and $n = \frac{1}{3}$ for the SEOS. The use of values $A = 0.048$ and $n = 0.323$ [*Anderson*, 1967*a*] as in *Ahrens et al.* [1969] will yield a somewhat higher zero-pressure density of ~3.80 g/cm^3. We conclude from these results that garnet of the majorite structure with a zero-pressure density of ~3.67 g/cm^3 is probably forming under shock conditions above ~135 kb in the present experiments and under similar pressures in the earth's mantle [*Ringwood*, 1970]. The observations of this mineral in shocked pyroxenes of similar composition indicate exposure to shock pressures of at least this magnitude.

Acknowledgments. The research was supported by the National Science Foundation under GA-12703 and the National Aeronautics and Space Administration under NGL05-002-105. We appreciate the invaluable technical support of John L. Lower and David Johnson, the assistance of Rex V. Gibbons, Arden L. Albee, Earl K. Graham, and Arthur Chodos in analyzing our specimen, and G. J. Wasserburg and Leon Thomsen for critical comments. We also thank Friedrich Horz and his colleagues at the Lunar Science Institute for their hospitality and the opportunity to present this work to a critical audience.

The publication was, in part, supported by NASA contract 09-051-001.

REFERENCES

Ahrens, T. J., D. L. Anderson, and A. E. Ringwood, Equation of state and crystal structure of high pressure phases of shocked silicates and oxides, *Rev. Geophys., 7*, 667–707, 1969.

Ahrens, T. J., J. H. Lower, and P. L. Lagus, Equation of state of forsterite, *J. Geophys. Res., 76*, 518–528, 1971.

Akimoto, S., High pressure synthesis of a 'modified' spinel and some geophysical implications, *Phys. Earth Planet. Interiors, 3*, 189–195, 1970.

Akimoto, S., and Y. Syono, High-pressure decomposition in the system $FeSiO_3$-$MgSiO_3$, *Phys. Earth Planet. Interiors, 3*, 186–188, 1970.

Akimoto, S., T. Katsura, Y. Syono, H. Fujisawa, and E. Komada, Polymorphic transition of pyroxenes $FeSiO_3$ and $CoSiO_3$ at high pressures and temperatures, *J. Geophys. Res., 70*, 5269–5278, 1965.

Anderson, Don L., A seismic equation of state, *Geophys. J., 13*, 9, 1967*a*.

Anderson, Don L., Phase changes in the mantle, *Science, 157*, 1165–1173, 1967*b*.

Anderson, Don L., and H. Kanamori, Shock-wave equations of state for rocks and minerals, *J. Geophys. Res., 73*, 6477–6502, 1968.

Anderson, D. L., C. Sammis, and T. Jordan, Composition of the mantle and the core, in *Proceedings of the Francis Birch Symposium, April 1970*, McGraw-Hill, New York, to be published in 1971.

Birch, F., Density and composition of the mantle and core, *J. Geophys. Res., 69*, 4377–4388, 1964.

Binns, R. A., $(Mg, Fe)_2SiO_4$ spinel in a meteorite, *Phys. Earth Planet. Interiors, 3*, 156–160, 1970.

Chao, E. C. T., O. B. James, J. A. Minkin, J. A. Boreman, E. D. Jackson, and C. B. Rayleigh, Petrology of unshocked crystalline rocks and evidence of impact metamorphism in Apollo 11 returned lunar sample, in *Proceedings of the Apollo 11 Lunar Science Conference, Houston,*

Texas, Geochim. Cosmochim. Acta. Suppl. 1, vol. 1, edited by A. A. Levinson, pp. 287–314, Pergamon, New York, 1970.

Clark, S. P., and A. E. Ringwood, Density distribution and constitution of the mantle, *Rev. Geophys., 2,* 35–88, 1964.

Davies, G., and D. L. Anderson, Revised shock-wave equations of state for high-pressure phases of rocks and minerals, *J. Geophys. Res., 76,* 2617–2627, 1971.

Deer, W. A., R. A. Howie, and J. Zussman, *An Introduction to the Rock Forming Minerals,* p. 112, Wiley, New York, 1966.

Gaffney, E. S., and T. J. Ahrens, Stability of mantle minerals from lattice calculations and shock-wave data, *Phys. Earth Planet. Interiors, 3,* 205–212, 1970.

James, O. B., Shock and thermal metamorphism of basalt by nuclear explosion, Nevada Test Site, *Science, 166,* 1615–1620, 1969.

Kumazawa, M., The elastic constants of single-crystal orthopyroxene, *J. Geophys. Res., 74,* 5973–5980, 1969.

Linde, R. K., and D. N. Schmidt, Shock propagation in nonreacting porous solids, *J. Appl. Phys., 37,* 3259–3271, 1966.

Mao, H., The pressure dependence of the lattice parameters and volume of ferromagnesium spinels, and its implications to the earth's mantle, Ph.D. thesis, University of Rochester, New York, 1967.

McQueen, R. G., S. P. Marsh, and J. N. Fritz, Hugoniot equation of state of twelve rocks, *J. Geophys. Res., 72,* 4999–5036, 1967.

McQueen, R. G., S. P. Marsh, J. W. Taylor, J. N. Fritz, and W. J. Carter, The equation of state of solids from shock wave studies, in *High Velocity Impact Phenoma,* edited by R. Kinslow, pp. 294–419, Academic, New York, 1970.

Ryzhova, T., K. S. Aleksandrov, and V. M. Korobkova, The elastic properties of rock-forming minerals, 5, Additional data on silicates, *Izv. Acad. Sci., USSR, Phys. Solid Earth,* no. 2, 111–113, 1966.

Ringwood, A. E., Phase transformations and the constitution of the mantle, *Phys. Earth Planet. Interiors, 3,* 109–155, 1970.

Ringwood, A. E., and A. Major, High-pressure transformations in pyroxenes II, *Earth Planet. Sci. Lett., 5,* 76–78, 1968.

Robie, R. A., and D. R. Waldbaum, Thermodynamic properties of minerals and related substances at 298.15°K (25.0°C), and one atmosphere (1.013 bars) pressure and at higher temperatures, *U.S. Geol. Survey Bull. 1259,* 1968.

Smith, J. V., and B. Mason, Pyroxene-garnet transformation in Coorara meteorite, *Science, 168,* 832–833, 1970.

Trunin, R. F., V. I. Gon'shakova, G. U. Simakov, and N. E. Galdin, A study of rocks under the high pressures and temperatures created by shock compression, (in Russian), *Izv. Acad. Sci., USSR, Phys. Solid Earth,* no. 9, 1–12, 1965.; Engl. transl. no. 9, 579–586, 1966.

Walsh, J. M. and Russell H. Christian, Equation of state of metals from shock wave measurements, *Phys. Rev., 97,* 1544–1556, 1955.

Wang, C., Phase transitions in rocks under shock compression, *Earth Planet. Sci. Lett., 3,* 107, 1967.

(Received January 7, 1971;
revised March 18, 1971.)